JOURNAL OF PROPULSION AND POWER
Vol. 26, No. 3, May–June 2010

Dynamic Simulation of a Space Reactor System with Closed Brayton Cycle Loops

Mohamed S. El-Genk,* Jean-Michel P. Tournier,† and Bruno. M. Gallo‡
University of New Mexico, Albuquerque, New Mexico 87131

DOI: 10.2514/1.46262

A dynamic simulation model for space reactor power systems with multiple closed Brayton cycle loops for energy conversion is developed and demonstrated for a startup transient. The simulated power system employs a submersion-subcritical safe space *S^4* reactor with a negative temperature reactivity feedback and has no single-point failures in reactor cooling and energy conversion. The *S^4* reactor core is divided into three hydraulically independent sectors, and each sector has a separate closed Brayton cycle loop that is thermal-hydraulically coupled to a circulating liquid NaK-78 secondary loop with two water heat pipe heat rejection radiator panels. Each closed Brayton cycle loop has a Brayton rotating unit designed and optimized for high thermal efficiency and low specific mass (1.16 kg/kW$_e$). The reactor coolant and the closed Brayton cycle working fluid is a He–Xe binary gas mixture with a molecular weight of 40 g/mol. Results are presented for a startup transient of the *S^4* closed Brayton cycle power system to full-power operation at a reactor thermal power 471 kW$_{th}$, a Brayton rotating unit shaft speed of 45 krpm, and turbine and compressor inlet temperatures of 1149 and 400 K, respectively. At these conditions, the nominal electrical power and thermal efficiency of the power system are 130.8 kW$_e$ and 27.8%.

Nomenclature

C	=	compressor
m	=	mass flow rate, kg/s
m^*	=	normalized mass flow rate, kg/s, $m^* = m\,(P_{\text{ref}}/P_{o,\text{in}})\sqrt{T_{o,\text{in}}/T_{\text{ref}}}$
P	=	pressure, Pa; electrical power, kW$_e$
P_{ref}	=	reference pressure, 0.4 MPa
T	=	temperature, K; turbine
T_{ref}	=	reference temperature, 400 K
x	=	bleed fraction of working fluid at exit of Brayton rotating unit compressor
η	=	thermal or polytropic efficiency, %
π	=	pressure ratio
ω	=	Brayton rotating unit shaft rotation speed, rad/s
ω^*	=	normalized shaft rotation speed, rad/s, $\omega^* = \omega\sqrt{T_{\text{ref}}/T_{o,\text{in}}}$

Subscripts

C	=	compressor
e	=	electric
G	=	generator
in	=	turbine or compressor inlet
o	=	stagnation or total
P	=	polytropic
Rx	=	reactor
Sec	=	reactor sector, or BRU turbine inlet
sys	=	power system
th	=	thermal
T	=	turbine

Received 6 July 2009; revision received 30 November 2009; accepted for publication 30 November 2009.

*Regents' Professor of Chemical, Nuclear, and Mechanical Engineering, Director, Institute for Space and Nuclear Power Studies, School of Engineering, MSC01 1120. Associate Fellow AIAA.

†Research Assistant Professor, Chemical and Nuclear Engineering Department, Institute for Space and Nuclear Power Studies, MSC01 1120. Member AIAA.

‡Former Research Assistant, Chemical and Nuclear Engineering Department, Institute for Space and Nuclear Power Studies, MSC01 1120.

I. Introduction

SPACE reactor power systems are enabling to future space exploration missions requiring 100 s to 1000 s kW$_e$, to where the solar option is impractical or nonexistent. In addition to their compactness and low specific mass (30–50 kg/kW$_e$), these power systems could operate continuously or intermittently with multiple startups and shutdowns for 10–15 years, or even longer. They also could provide surface power for lunar and Mars outposts and operate high specific impulse (5000–15,000 s) ion thrusters for fast travel to distant planets in the solar system. Operation reliability and long life of space reactor power systems could be assured by operating at reasonable temperatures <1200 K and moderate fission power levels and avoiding single-point failures in reactor cooling and energy conversion. At such temperatures, conventional steel (<900 K) and nickel-based steel alloys could be used for the structure, and the fuel swelling and fission gas release are low.

For convectively cooled space reactors, an avoidance of single-point failures could be accomplished by 1) designing the reactor core with 3–6 sectors that are hydraulically independent but thermally and neutronically coupled, and 2) thermal-hydraulically coupling each reactor sector to a separate energy conversion loop or modules with a separate heat rejection loop and/or heat pipe radiator panels [1–10]. Thus, a pipe break in one of the energy conversion loops would not compromise the system operation and mission because the reactor fission power would be reduced, and the power generated in the sector with a failed energy conversion loop would be conducted to adjacent sectors where it is removed by the circulating liquid metal or gas coolant in these sectors. Single-point failures in space reactor power systems can also be avoided by using a liquid-metal heat pipe's cooled reactor coupled to a multitude of energy conversion loops or modules [6].

Dynamic simulation of the operation of space reactor power systems, although complex, is an effective and desirable capability for investigating the effect of the design of different components on the power system performance and/or integration, while minimizing its total size and mass. Transient simulation models of integrated space reactor power systems can also be used to develop strategies for adaptive control and autonomous operation [11–13] that could be implemented into software. Such a capability would enable space

reactor power systems for deep space missions, beyond Mars, to detect and recognize a component malfunction and alter the operation of the reactor and the system to mitigate long-term consequences.

A number of dynamic simulation models of different space reactor power systems have been developed [4,14–19]. The Space Nuclear Power Systems Analysis Model for the SP-100 system [20,21], with a fast-spectrum reactor heat source and multiple circulating liquid lithium loops with thermoelectric-electromagnetic (TEM) pumps and Silicon-Germanium (SiGe) thermoelectric (TE) conversion modules, had been developed and successfully validated by comparing predictions with reported simulation results by General Electric Company [15–17]. Actual system operation parameters were not available. This transient system model was used to investigate the performance of the SP-100 system during startup, following a failure of multiple TEM pumps, and after shutdown [14–17].

A dynamic simulation model had also been developed for the former Soviet Union's TOPAZ-II space reactor power system and successfully benchmarked using actual system performance and test data [18,19]. The predictions were within a few percent of the measured system parameters such as the load voltage and electric power, the circulation rate of the NaK-78 working fluid, etc. [18,19]. The TOPAZ-II reactor had an epithermal neutron energy spectrum, in-core thermionic fuel elements (TFEs), and stainless steel structure and was cooled by circulating liquid NaK-78. It operates at a nominal steady-state power of $\sim$125 kW_{th} and exit temperature of $\sim$800 K, however, the in-core TFEs operate at an emitter surface temperature of 1800–1990 K and are loaded with highly enriched (95%) UO_2 fuel pellets. At steady-state, full-power operation the TOPAZ-II power system, rated for an operation life of $<$2 years, nominally generates a total of $\sim$5.5 kW_e at a load voltage of $\sim$28 VDC.

Recently, a dynamic simulation model (DynMo-TE) has been developed and used to investigate the transient operation of space reactor power systems having a circulating liquid metal-cooled reactor and six pairs of primary and secondary coolant loops with TEM pumps, SiGe thermoelectric energy conversion modules, and liquid-metal heat pipe radiator panels [4]. Each primary and secondary liquid metal loop has a bellows-type accumulator for controlling the loop pressure and accommodating the changes in the volume of the liquid metal working fluids with temperature during transient operation. Different types of liquid metal coolant/working fluid could be used in the primary and secondary loops for improving the system performance and transient response [4].

The simulated power system using DynMo-TE has no single point failures in reactor cooling and energy conversion. It employs a sectored compact reactor (SCoRe) with liquid-metal heat pipes dividing the reactor core into six equal sectors [5,7]. The reactor core sectors are thermally and neutronically coupled, but hydraulically independent. Each sector has a separate pair of primary and secondary loops and each loop has a separate EM pump and a bellows-type accumulator [22]. A SiGe power conversion assembly (PCA) and a thermoelectric conversion assembly (TCA) are conductively coupled to each pair of primary and secondary loops to establish the temperature differential for TE energy conversion [4]. Each secondary loop has two separate rubidium heat pipes radiator panels for heat rejection [23]. The primary loops of the SCoRe-TE space power system transports the thermal power generated in the reactor sectors by 1026 uranium nitride (UN) fuel pins (or 171 fuel pins per sector) to the PCAs and to the electromagnetic pump's TCAs. At steady-state, full-power operation, the SCoRe-TE system with circulating liquid lithium secondary and primary loops nominally supplies a total of 111.5 kW_e to the electrical load at 450 VDC [4].

The constituent equations in DynMo-TE [4] are solved using the SIMULINK® platform [24], an interactive graphical environment that allows rapid development of a library of blocks of the system components. These components are easily replaced or exchanged in the system model. Through MATLAB®, SIMULINK® accesses an extensive range of tools for numerical computation, time integration, algorithm development, and data visualization and analysis. The DynMo-TE had been used to investigate the transient operation and startup of the SCoRe-TE space reactor power system and its load-following characteristics. It also was used to investigate the effect of the type of the circulating liquid metal coolant (Li, Na, or NaK-78) in the primary and secondary loops on the power system performance and transient response [4]. While successfully demonstrating the dynamic simulation of such a complex space reactor power system, the simulation results could not be validated due to the absence of actual system data.

Recently, DynMo-TE has been used to simulate a startup transient and the steady-state operation to the end of the six-year operation life of the SCoRe-NaK-TE space reactor power system. This power system used circulating liquid NaK-78 in the primary and secondary loops [25]. The reactor and power system had a stainless-steel structure because it operates at a reactor exit temperature of $\sim$900 K, a major advantage for reducing the development cost and enhancing the operation reliability of the power system. The SCoRe-NaK-TE power system nominally generates $\sim$37.1 kW_e at a load voltage of $\sim$300–312 VDC to support a satellite in 1000–3000 km earth orbits for a civilian global air and sea traffic control [25]. These orbits within the inner Van Allen radiation belt have estimated decay lives of 700–1000 years and could be safely used for end-of-life storage of the reactor and the power system.

Though future uses of space reactor power systems may be limited to enabling deep space exploration missions, this civilian mission in Earth orbit is justified because solar photovoltaic cells

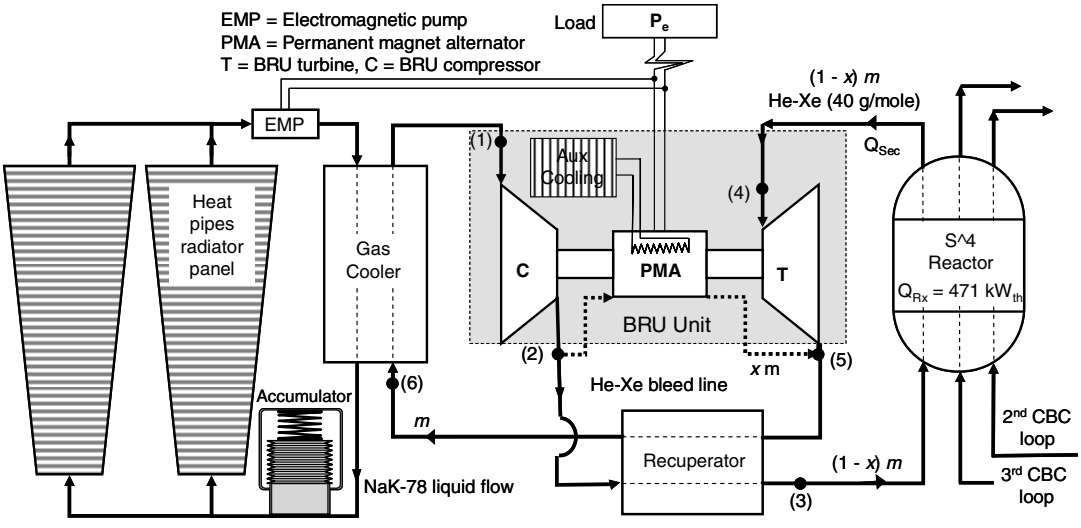

Fig. 1 A layout of one CBC loop in the *S* ^ 4 CBC space reactor power system.

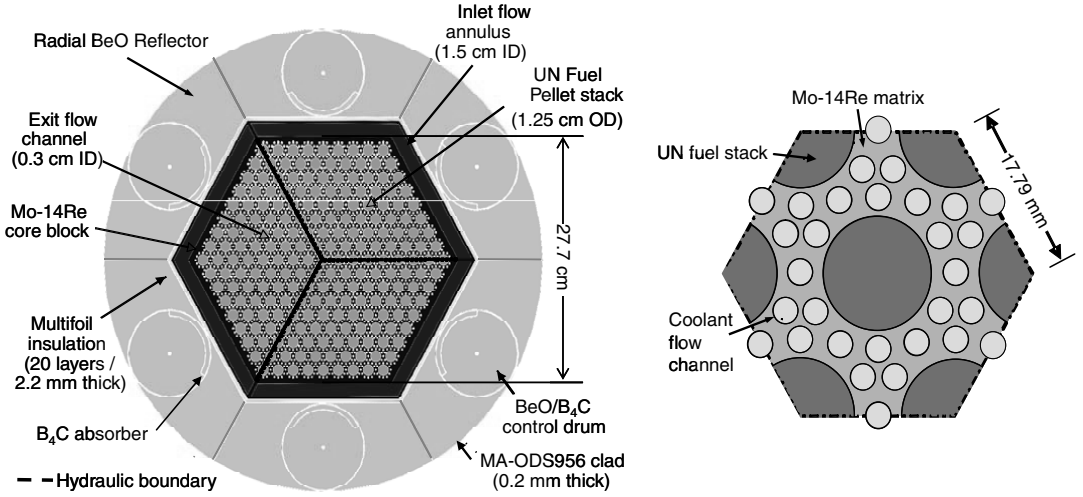

a) Radial cross-section of S^4 reactor

b) Fuel elements – coolant channels unit cell

Fig. 2 Radial cross sections of *S* ^ 4 reactor [8,9].

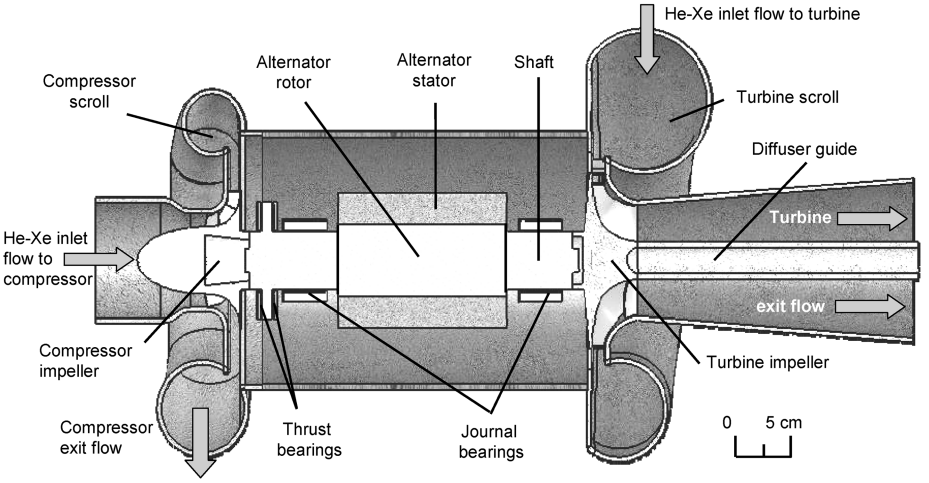

a) A cut-away view

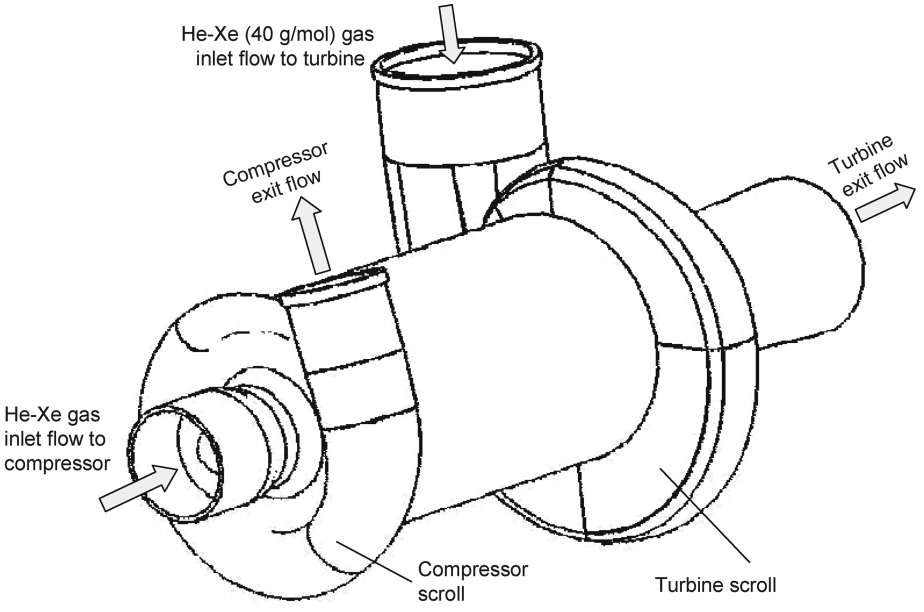

b) An isometric view

Fig. 3 Cutaway and isometric views of the UNM-BRU-1.

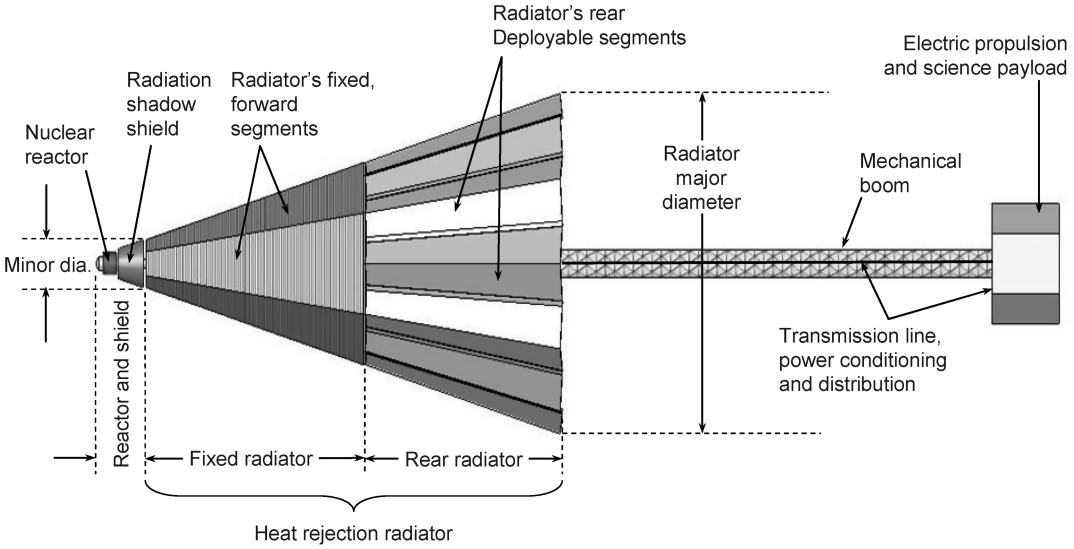

Fig. 4 $S^{\wedge}4$ CBC space reactor power system, fully deployed.

would not survive the high-energy ionizing particles (protons and electrons) trapped within the Van Allen radiation belts [25] and the solar panels would be huge, requiring high-capacity storage batteries and a large amount of propellant for orbit adjustments.

This paper develops and demonstrates a dynamic simulation model for space reactor power systems with closed Brayton cycle (CBC) energy conversion (DynMo-CBC). Due to the absence of actual operation data to validate the current predictions, the primary emphasis is not on the accuracy of the results, but rather on extending and demonstrating the modeling capabilities to a complex space reactor power system with multiple CBC energy conversion loops and no single point failures. The simulated power system (Fig. 1) employs a gas-cooled, submersion-subcritical safe space ($S^{\wedge}4$) reactor heat source (Fig. 2). The reactor core is divided into three sectors that are hydraulically independent, but thermally and neutronically coupled [8–10] (Figs. 2a and 2b). The DynMo-CBC and the constituent models of the $S^{\wedge}4$-CBC power system components are briefly described in this paper, and the simulation results of a startup transient to a full-power, steady-state operation are presented and discussed.

In the $S^{\wedge}4$-CBC power system, each of the three sectors in the $S^{\wedge}4$ reactor core is thermal-hydraulically coupled to a separate CBC loop with a Brayton rotating unit (UNM-BRU-1), designed for high thermal efficiency and low specific mass (Fig. 3) [26]. The UNM-BRU-1 unit employs a permanent magnet alternator (PMA) with an efficiency of 95%. It has been optimized for operating at peak thermal efficiency and electrical power of 28.5% and 44.7 kW_e, respectively, when operating at turbine and compressor inlet temperatures of 1149 K and 400 K, respectively, shaft rotation speed of 45 krpm, and input thermal power to the turbine $Q_{sec} = 157\ kW_{th}$ [26]. The corresponding reactor thermal power is 471 kW_{th}, divided equally among the three core sectors [8–10].

For waste heat rejection, each of the three CBC loops of the $S^{\wedge}4$-CBC power system (Fig. 4) is thermally coupled to a circulating liquid NaK-78 secondary loop with two water heat pipe radiator panels. Each radiator panel consists of a forward fixed segment and two rear deployable segments. The three segments are hydraulically connected in parallel in order to reduce the pressure losses in the NaK secondary loops, enhance performance, and reduce the size of the panels. Details of the design and performance optimization of the water heat pipe radiator panels are given elsewhere [27] (Fig. 5). The liquid NaK in the three heat rejection loops is circulated using alternating linear induction pumps (ALIPs) [28]. Each ALIP consumes ~1.1 kW_e, decreasing the net electrical power supplied to the electrical load by each UNM-BRU-1 by that amount to 43.6 kW_e. Thus, the electrical power, provided by the $S^{\wedge}4$-CBC power system at steady-state, full-power operation (Figs. 1 and 4) is ~130.8 kW_e at a thermal efficiency of ~27.8% [26].

The fully deployed $S^{\wedge}4$-CBC space power system is shown in Fig. 4. The radiation shadow shield behind the reactor protects the electronic and electrical components within the cavity of the deployed radiator. The reactor coolant and CBC working fluid in the $S^{\wedge}4$-CBC space power system is a He–Xe binary gas mixture with a molecular weight of 40 g/mol. This high molecular weight working fluid has a comparable convective heat transfer coefficient to that for helium (4 g/mol), which is significantly higher than those for pure krypton or xenon [29]. In addition, it effectively reduces the size and mass of the UNM-BRU-1 [26,29].

II. $S^{\wedge}4$ Reactor

The submersion-subcritical safe space ($S^{\wedge}4$) reactor [8–10] generates up to 471 kW_{th} of steady-state thermal power for up to 12 years, shared equally among the three sectors of the core. Thus, each sector nominally generates up to 157 kW_{th}. The $S^{\wedge}4$ reactor has a hexagonal, Mo-14Re (molybdenum with 14 wt % rhenium) solid core with cylindrical cavities loaded with uranium nitride (UN) fuel pellets and surrounded by He–Xe coolant channels (Figs. 2a and 2b). There are a total of 217 UN fuel stacks and 1977 coolant channels in the reactor core. The 1.25 cm diameter UN fuel stacks are arranged in a triangular lattice with a pitch of 1.779 cm. The coolant channels are 3 mm in diameter. Each fuel stack is surrounded by 12 channels but effectively cooled by 9 channels (Figs. 2a and 2b).

Iridium foils (0.1 mm thick) are wrapped on the outside of the UN fuel stacks in the cavities to enhance heat conduction to the solid core block and suppress the diffusion of solid fission products from the fuel pellets to the core block. Following a launch abort accident, in order to ensure that the bare core of the $S^{\wedge}4$ reactor remains sufficiently subcritical when submerged in wet sand and flooded with seawater, 1.95 wt % ^{151}EuN is added to the 95 wt % enriched UN fuel pellets in the core. The ^{151}EuN neutron poison minimally affects the reactivity of the fast neutron energy spectrum, $S^{\wedge}4$ reactor during nominal operation. However, it effectively absorbs thermal neutrons produced in the submerged and flooded core during a launch abort accident, keeping it subcritical [8–10].

As indicated earlier, the $S^{\wedge}4$-CBC space power system, with a reactor core comprised of three hydraulically independent sectors, each with a separate CBC loop, avoids single point failures in reactor cooling and energy conversion. The fission power generated in a reactor sector connected to a failed CBC loop transports by conduction and/or radiation to the metal dividers, then to the two adjacent sectors, where it is removed by forced convection of the circulating He–Xe gas in these sectors. The high thermal conductivity of the Mo-14Re solid core of the $S^{\wedge}4$ reactor (>65 $W/m \cdot K$) facilitates the transfer of the generated fission heat from the sector experiencing a loss of cooling to the adjacent sectors by conduction.

Thus, following a loss-of-cooling, or a pipe break in one of the CBC loops, the $S^{\wedge}4$-CBC power system could continue to operate with only two functioning CBC loops, but at a lower power (Figs. 1 and 6), thus enhancing the system and mission reliability.

III. Dynamic Simulation Model

The DynMo-CBC model of the $S^{\wedge}4$-CBC space power system is based on the SIMULINK® platform [24]. DynMo-CBC (Fig. 6) couples the physical models of the various components in the power system (Fig. 1) using a thermodynamic model of the CBC loop. This transient system model incorporates the following: 1) an $S^{\wedge}4$ reactor model, 2) thermal-hydraulics models of the CBC and the NaK-78 heat rejection loops (Fig. 1), 3) an integrated model of the UNM-BRU-1 (Fig. 3) [26], 4) a BRU proportional integral differential (PID) controller, 5) a thermodynamics model of the CBC loops, 6) models of the ALIPs and the liquid-metal, bellows-type accumulators in the NaK-78 heat rejection loops, and 7) a thermal-hydraulics model of the segmented radiator panels and the water heat pipes (Fig. 5) [27]. The salient features of these models are described briefly next.

$S^{\wedge}4$ Reactor Model: It couples a six-group kinetics submodel to a thermal-hydraulics model of the reactor core (Fig. 6). The former calculates the reactor's fission power subject to the magnitude of the external reactivity insertion at a user specified rate, and accounts for the reactivity feedbacks in the reactor due to temperature, the depletion of fissile, and the accumulation of fission products in the UN fuel. The reactor's thermal-hydraulics model calculates the average temperatures of the UN fuel, the Mo-Re solid core block, and the circulating He–Xe binary gas mixture through coolant channels in the reactor core. These temperatures are determined by solving the coupled momentum and energy balance equations in the reactor core, subject to the reactor's thermal power provided by the reactor kinetics submodel. This is in addition to the reactor inlet temperature and the flow rate of the returning He–Xe from the recuperators in the three CBC loops, calculated using the coupled thermal-hydraulics/ thermodynamic models of CBC loop (Figs. 1 and 6).

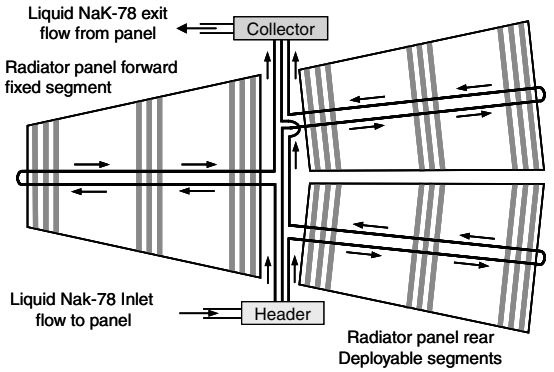

a) Hydraulic coupling of a radiator panel segments

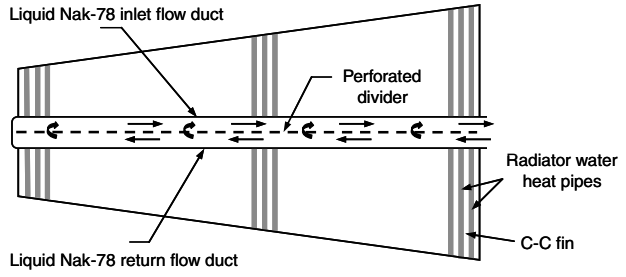

b) Radiator panel forward fixed segment (1 of 6)

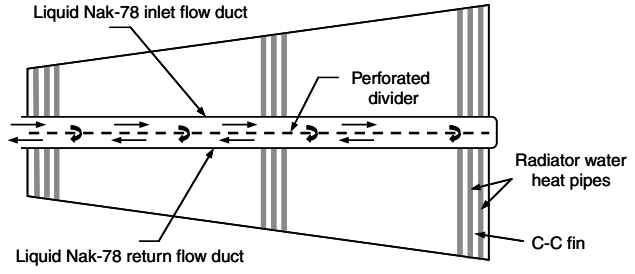

c) Radiator panel rear deployable segment (1 of 12)

Fig. 5 Layout and liquid NaK-78 flow in a radiator panel and segments.

CBC Loop Model: The CBC loop model thermal-hydraulically couples those of the various loop components: the gas cooler, recuperator, reactor, and the UNM-BRU-1 (Figs. 1, 3, and 6). The flow channels in the reactor, recuperator, and the gas cooler are discretized into small axial control volumes, and the CBC loop model solves the transient mass, momentum, and energy balance equations in each control volume and ensures that the overall momentum and energy balances in the CBC loop are satisfied. The CBC loop model accounts for the transient changes in the pressure and the thermal inertia of the He–Xe working fluid, the connecting piping, the nuclear reactor, the recuperator, and the gas cooler. The energy balance equation of the CBC loop accounts for the parasitic heat losses.

The volumetric thermal expansion and pressure of the circulating NaK-78 liquid in the heat rejection loops are controlled by the accumulators [22] in these loops (Figs. 1 and 6). The coupled thermal-hydraulics and thermodynamic models of the CBC loop determine the flow rate of the He–Xe coolant in the reactor core sectors and the values of the pressure, pressure losses, and temperature in the reactor and other components of the CBC loop. The thermal-hydraulics model of the CBC loop is coupled to that of the circulating liquid NaK-78 in the heat rejection loop in the gas-cooler (Figs. 1 and 6).

Heat Rejection Loop Model: This model (Figs. 1 and 6) thermal-hydraulically couples the models of the various components in the heat rejection loop (the gas cooler, accumulator, ALIP, and the segments and the water heat pipes of the radiator panels), and accounts for the parasitic heat losses in the loop. In addition to the temperatures throughout the heat rejection loop, this integrated model also calculates the circulation rate of the liquid NaK-78 during various operation transients of the $S^{\wedge}4$-CBC power system and the average surface temperature of the radiator panels for heat rejection.

UNM-BRU-1 Model and the PID Controller: The UNM-BRU-1 model couples the submodels of the centrifugal flow compressor, the radial inflow turbine, the rotating shaft (Fig. 3) [26], and the permanent magnet alternator. The electrical efficiency of the alternator is assumed $= 95\%$. These submodels account for the various enthalpy losses in the turbine and the compressor and the shaft mechanical losses as functions of the shaft rotation speed and input thermal power and temperature to the turbine [26]. The UNM-BRU-1 submodel is integrated into the CBC loop thermodynamic model that solves the transient mass, momentum, and energy balance equations and accounts for the changes in the thermal masses of the UNM-BRU-1 unit and other CBC loop components. The submodel of the UNM-BRU-1 unit incorporates performance maps for the compressor and the turbine. These maps are used to speed up the simulation and ensure sufficient surge margin for the compressor during the startup transient of the $S^{\wedge}4$-CBC power system [26]. They are used to calculate the pressure ratios and polytropic efficiencies of the compressor and turbine as functions of the flow rate, the inlet temperature and pressure of the He–Xe working fluid (40 g/mol), and the shaft rotational speed.

The BRU shaft submodel accounts for the turbine and compressor disk windage losses, as well as the windage losses in the electrical alternator, the bearings, and at the exposed surface of the rotating shaft [26]. The shaft rotation speed in the UNM-BRU-1 units is maintained using a PID controller. It regulates the applied voltage (and consequently the electrical power) to the starter motors during

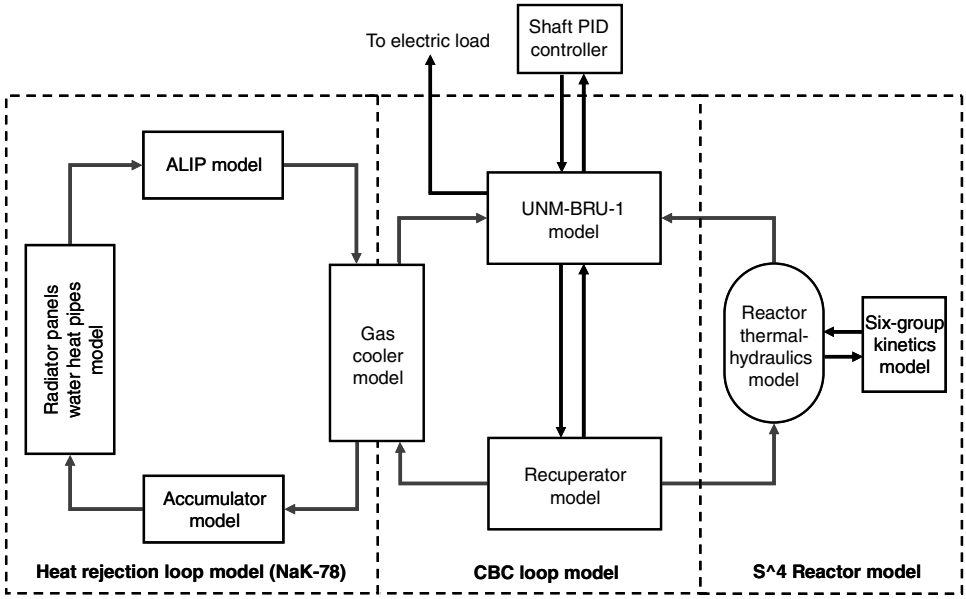

Fig. 6 Building blocks of DynMo-CBC for *S^4*-CBC space reactor power system.

the power system startup and until the net mechanical work of the BRU shaft becomes positive. Thereafter, the PID controller maintains the shaft rotation speed constant at the user specified value. At full-power steady-state operation of the *S^4*-CBC space power system, the shaft rotation speed for the three UNM-BRU-1 units is kept constant at 45 krpm.

Accumulator Model: The model of the bellows-type accumulators in the circulating liquid NaK-78 heat rejection loops (Figs. 1 and 6) [22] accounts for the volume changes in the NaK-78 liquid in the loop and the associated changes in the stiffness of the metal spring and the bellows, and the pressure of the inert gas in the accumulator as functions of the NaK-78 temperature. This model also accounts for the changes in the thermal inertia of the liquid NaK-78 in the loop and in the accumulator bellows, metal spring, and the chamber wall with temperature. The coupled hydrodynamic model of the accumulator and the thermal-hydraulics model of the circulating liquid NaK-78 in the heat rejection loop calculate the average temperature of accumulator and the pressure of the liquid NaK in the loop.

Radiator Panel Thermal-Hydraulics Model: This model hydraulically couples the circulating liquid NaK-78 in the three segments (one forward and two in the rear) of the radiator panels. It also thermally couples the circulating NaK to the water heat pipes in the radiator panel's segments (Fig. 5). This thermal-hydraulic model of the radiator panel discretizes the inlet and return flow ducts in each panel segment (Fig. 5) into small axial control volumes. It then calculates the rate of heat transfer by forced convection from the circulating NaK-78 to the water heat pipes in the radiator panels. These heat pipes have carbon-carbon (C-C) armor and C-C fins [23,27]. In each control volume of the NaK flow ducts in the panel segments, this model solves the coupled momentum and energy balance equations of the circulating liquid NaK-78 and calculates the changes in its temperature and pressure. It also calculates the pressure losses in the heat rejection loop and across the perforated dividers between the inlet and exit flow in the ducts of the radiator panel segments (Fig. 5). This model calculates the change in the flow rate of the liquid NaK-78 along these flow ducts in the radiator panel segments, and both the local radiation view factor and the effective fin efficiency for rejecting the waste heat into space. The radiator panel model that is coupled to a transient water-heat pipe model calculates the water vapor flow rate, as well as the temperatures and pressure drops in the heat pipes and in the condenser structure, which transports heat to the base of the C-C fins [23,27]. The transient water heat pipe model also calculates the sonic, capillary, entrainment, and incipient boiling limits.

The developed DynMo-CBC model (Fig. 6) in this work is rather involved and complex. It is used in this paper to demonstrate its capabilities for simulating the startup transient of the *S^4*-CBC space power system (Fig. 1) from an initial temperature of 400 K. The primary emphases have been on demonstrating the functionality of this system model rather than on the accuracy of the results, which can only be validated when actual system data becomes available. Nonetheless, while the UNM-BRU-1 model has been successfully validated [26], extreme care has been taken to ensure a sound and credible modeling approach and minimize uncertainties. This will be discussed in further detail later.

The obtained performance results are presented and discussed in the next section. The calculated system operation parameters using DynMo-CBC are: 1) the total reactivity, thermal power, and temperatures of the *S^4* reactor, 2) the mechanical work of the UNM-BRU-1 shaft and the electrical power generated by and the corresponding thermal efficiency of the power system, 3) the flow rate of the He–Xe working fluid in the reactor sectors and CBC loops and of the He–Xe gas temperatures and pressures at different points of the CBC loops, 4) the pressure ratios and polytropic efficiencies of the UNM-BRU-1 turbine and compressor, and 5) the UNM-BRU-1 turbine and compressor works and net shaft work. In addition to the actual design, hardware dimensions, and material properties of the various CBC loop components, the input to DynMo-CBC includes the rate and magnitude of the external reactivity insertion into the reactor core during the power system startup transient and the UNM-BRU-1 shaft speed, which is maintained by the PID controller. The simulation capabilities of the transient, object-oriented, DynMo-CBC system model, developed based on the SIMULINK® platform [24], allow the user to replace individual system components relatively easily. This is particularly important because an optimum system for given requirements is not necessarily that made up of individually optimized components.

IV. Startup Simulation of *S^4* Closed Brayton Cycle Power System

At the beginning of the startup procedures (Fig. 7) of the *S^4*-CBC space power system, it is assumed to be at 400 K with the 12 radiator panels folded in the stowed launch configuration (Fig. 8a) (i.e., the heat rejection from the power system is nil). The parasitic heat losses from the power system to space are neglected in the startup simulation, because the piping and the components in the CBC loops are assumed to be well insulated. The detailed radiator design and performance results of the water heat pipe heat rejection radiator panels have been presented in [27], and are thus not included in this paper. The present startup simulation assumes an arbitrary equilibrium space sink temperature of 250 K and an effective surface

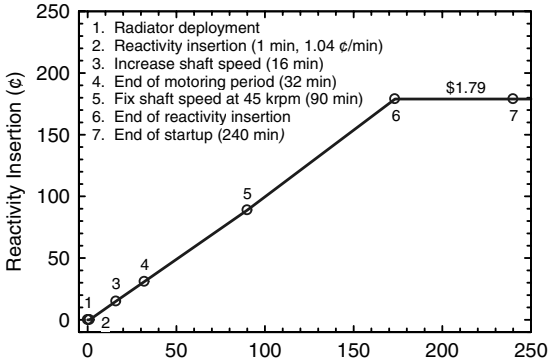

a)

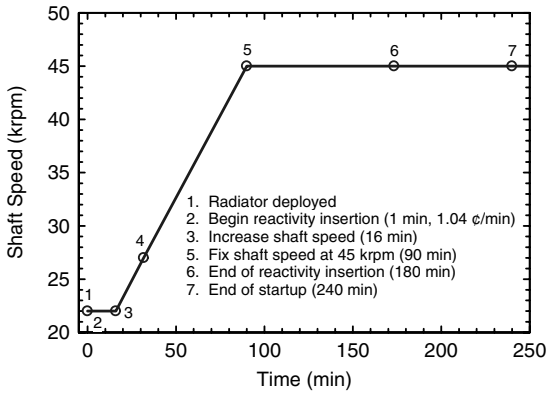

b)

Fig. 7 The startup procedures of the $S^{\wedge}4$-CBC space power system.

emissivity for the radiator panels of 0.85. Each CBC loop in the $S^{\wedge}4$-CBC power system (Figs. 1 and 6) is filled with 2.49 kg (or 62.2 moles) of He–Xe binary gas mixture (40 g/mol), which corresponds to an initial pressure in the CBC loops of 0.475 MPa. The inventory of the He–Xe working fluid in the three CBC loops of the power system does not change during the simulated startup transient of the $S^{\wedge}4$-CBC power system.

At nominal, full-power steady-state operation, the thermal power generated in the $S^{\wedge}4$ reactor is 471 kW_{th}, the UNM-BRU-1 shaft rotation speed is 45 krpm, the turbine and compressor inlet temperatures are 1149 K and 400 K, and the operating pressure at the exit of the compressor is 0.928 MPa. At these conditions, each UNM-BRU-1 generates 44.7 kW_e at a thermal efficiency of 28.5%. The estimated total mass of the UNM-BRU-1 unit is 51.78 kg [26], including 9.65 kg for the cobalt–samarium permanent magnet alternator, which results in a unit specific mass as low as ~1.16 kg/kW_e [26].

The calculated changes in the transient operation parameters during the startup of the $S^{\wedge}4$-CBC space power system are shown later in this section. With the radiator initially in the stowed configuration (Fig. 8a) and prior to initiating the reactivity insertion into the $S^{\wedge}4$ reactor by rotating the control drums in the radial beryllium oxide (BeO) reflector incrementally outward (Fig. 2a), the PID controller operates the starter motors, maintaining the rotation speed of the UNM-BRU-1 shaft steady at 22 krpm (Fig. 7b). At time zero of the startup procedures (point 1 in Fig. 7), the radiator panels begin deployment (Fig. 8b), a process that takes one minute to complete. After the 12 radiator panels are fully deployed, the control drums in the radial BeO reflector are rotated outward (Fig. 2a) to insert reactivity into the $S^{\wedge}4$ reactor core (point 2 in Fig. 7) at a constant rate of 1.04 ¢/ min. After 180 min into the startup transient (point 6 in Fig. 7a), the total reactivity inserted into the reactor core is +$1.79. The full startup procedures to reach steady-state, nominal full-power operation of the $S^{\wedge}4$-CBC power system takes an additional 60 min or a total of 4 h to complete (point 7 in Fig. 7).

After 16 min into the startup transient, the PID controller of the starter motors begins to increase the rotation speed of the UNM-BRU-1 shaft beyond 22 krpm, at a constant rate of 311 rpm/ min. The increased shaft speed increases the pressure ratio of the UNM-BRU-1 compressor and turbine and the mass flow rate of the He–Xe working fluid in the CBC loops of the $S^{\wedge}4$ power system. This phase ends when the shaft speed reaches 45 krpm, 90 min into the startup transient (point 5 in Fig. 7b). Thereafter, the PID controller maintains the shaft rotation speed constant at 45 krpm, even after the power system reaches full-power, steady-state operation.

The next sections present and discuss the calculated results demonstrating the changes in the various operation parameters of the $S^{\wedge}4$ reactor during the startup procedures delineated in Figs. 7a and 7b. These parameters include the total reactivity insertion into the $S^{\wedge}4$ reactor, the reactor thermal power and temperatures, the pressure ratios and polytropic efficiencies of the UNM-BRU-1 compressor and turbine, and the system pressures, electrical power to the load, and thermal efficiency.

A. Reactor Operation Parameters

The calculated transient values of the various operation parameters of the reactor and the $S^{\wedge}4$-CBC space power system during the startup procedures (Fig. 7) are presented in Figs. 9–15. Figure 9a shows the calculated changes in the external, total reactivity, and the temperature reactivity feedback in the $S^{\wedge}4$ reactor, while Figs. 9b and 9c present the calculated changes in the reactor thermal power and temperatures. The temperature feedback reactivity in Fig. 9a is the sum of those due to the UN fuel, the Mo-Re core block, and the

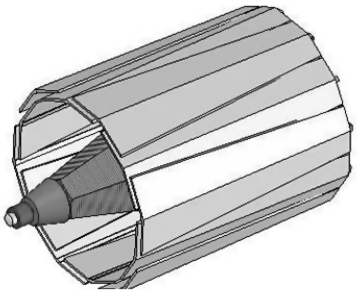

a) S^4-CBC power system in stowed configuration

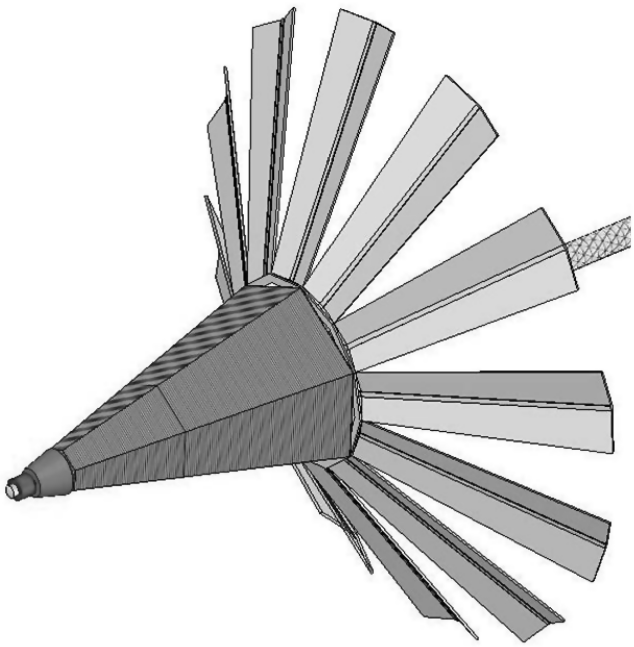

b) S^4-CBC power system during deployment

Fig. 8 Stowed and deploying configurations of $S^{\wedge}4$-CBC space power system.

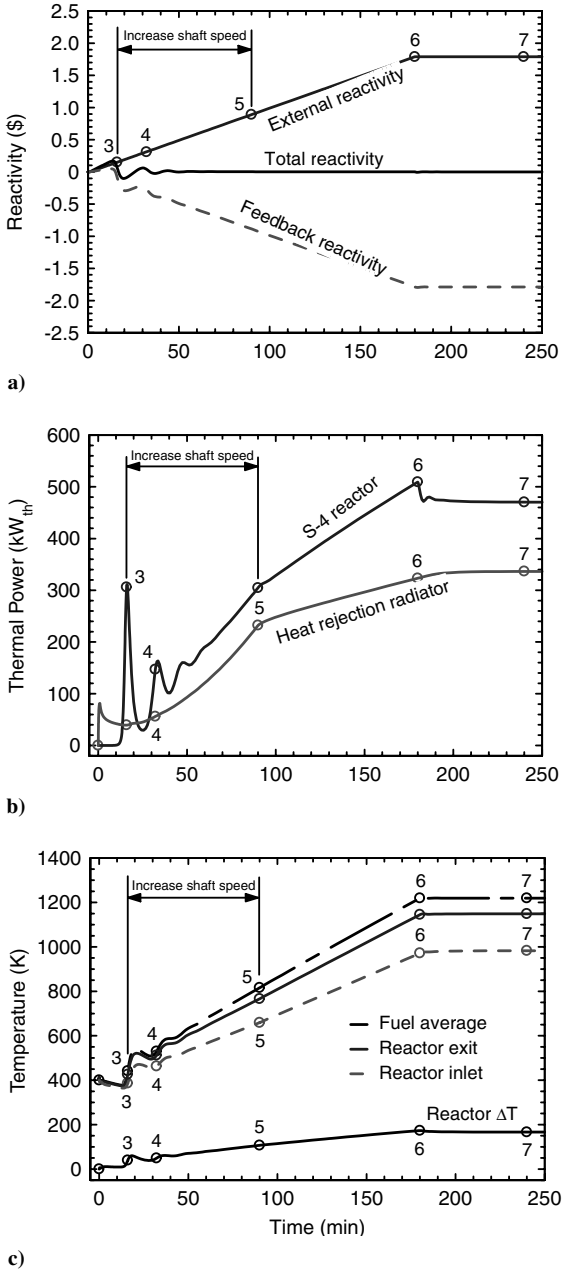

Fig. 9 Reactor operation parameters during the startup of $S^{\wedge}4$-CBC power system.

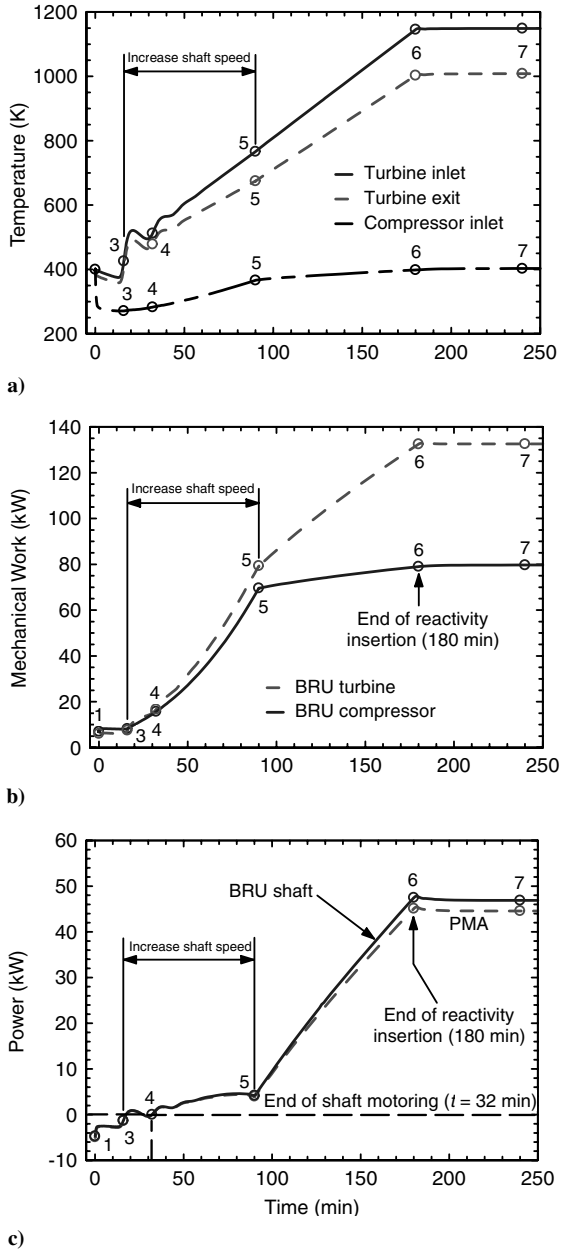

Fig. 10 UNM-BRU-1 parameters and shaft power during the startup of $S^{\wedge}4$-CBC power system.

He–Xe working fluid in the $S^{\wedge}4$ reactor core. The temperature-feedback reactivity coefficients for the fuel and Mo-Re core block are both negative, but the former is an order of magnitude larger. The temperature reactivity feedback coefficient of the He–Xe coolant is negligibly small. Thus, the temperature reactivity feedback in the $S^{\wedge}4$ core is essentially driven by the change in the average fuel temperature (Fig. 9c).

At full-power, steady-state operation the average fuel temperature is 155 K higher than the average temperature of the He–Xe binary gas coolant in the reactor. This large temperature difference is caused by the relatively low, forced convection heat transfer coefficient of the He–Xe binary gas mixture. The temperature drop through the boundary layer in the circular coolant channels in the $S^{\wedge}4$ core (Fig. 2b) is 140 K. The thermal resistance in the boundary layer is $\sim$100 times greater than that by conduction in the solid Mo-Re core structure. The sum of the radial average temperature drops in both the Mo-Re core structure and the UN fuel pellets is only 15 K, because of the relatively high thermal conductivities of these materials ($\sim$68 and 21.5 W/m $\cdot$ K, respectively). The rise in the temperature of the He–Xe gas flow through the nuclear reactor increases commensurate with the reactor thermal power and reaches its highest value of 166 K at steady-state, full-power operation of the $S^{\wedge}4$ reactor at 471 kW$_{th}$ (Figs. 9b and 9c).

During the first 16 min of the startup transient, the reactor thermal power increases rapidly to a peak of 306 kW$_{th}$ before decreasing again rapidly (Fig. 9b), as the average reactor temperature increases (Fig. 9c), decreasing the total reactivity in the reactor core (Fig. 9a) because of the negative temperature reactivity feedback. The reactor thermal power exhibits two subsequent peaks of 163 kW$_{th}$ and 161 kW$_{th}$, following the increase in the rotation speed of the UNM-BRU-1 shaft from 22 to 45 krpm (point 3 in Fig. 9). During the shaft speed ramp phase and after 60 min into the startup transient, the reactor thermal power increases almost linearly as the total external reactivity insertion into the $S^{\wedge}4$ reactor increases (point 5 in Fig. 9). After reaching a constant shaft speed of 45 krpm the reactor thermal power continues to increase linearly, but at a slightly lower rate to the end of the external reactivity insertion phase of the startup procedures (point 6 in Fig. 9).

Almost immediately after the full deployment of the radiator panels (Fig. 4 and points 1 and 2 in Fig. 7), the thermal power rejected

by the $S^{\wedge}4$-CBC power system increases rapidly to about 81 kW_{th} (Fig. 9b), decreasing the temperature at the inlet of the UNM-BRU-1 compressor to 275 K (point 3 in Fig. 10a). The turbine inlet temperature, however, decreases only slightly to 373 K (Fig. 10a). Subsequently, the inlet temperatures to the UNM-BRU-1 compressor and turbine increase monotonically with time during the startup procedures (Fig. 10a). This is because the reactor's thermal power increases significantly faster than the heat rejection rate of the 12 radiator panels of the $S^{\wedge}4$-CBC space power system (Fig. 9b).

B. Brayton Rotating Unit-1 Operation Parameters

After 32 min into the startup procedures of the $S^{\wedge}4$-CBC power system, the inlet temperature to the UNM-BRU-1 turbine increases to 512 K (Fig. 10a) and the shaft net mechanical power becomes zero, marking the end of the motoring phase of the UNM-BRU-1 units in the power system (Fig. 11). This is when the net mechanical power of the UNM-BRU-1 shaft becomes and stays positive. Beyond this time, the turbine mechanical power becomes increasingly higher than that demanded by the compressor after accounting for the shaft mechanical losses (Fig. 10) [26]. As shown in Fig. 10b, during the motoring phase of the UNM-BRU-1 units, the turbine mechanical power is initially lower than that required by the compressor, with the difference provided by the starter motors at the user-specified shaft speed to the PID controller.

At the beginning of the startup transient, the motoring power consumed by each of the startup motors of the UNM-BRU-1 unit is 4.9 kW_e. This is when the power system is at a uniform temperature of 400 K and the UNM-BRU-1 shaft is rotating at a constant speed of 22 krpm. The power consumed by the starter motor decreases rapidly to 2.8 kW_e following the deployment of the radiator panels (point 2 in Fig. 11), momentarily cooling the CBC loops (Fig. 10a). The cumulative energy consumption during the motoring phase of each UNM-BRU-1 is 2.76 MJ (Fig. 11). This energy is provided by the batteries onboard the spacecraft.

At the start of the ramp phase of the UNM-BRU-1 shaft speed, 16 min into the startup transient (point 3 in the figures), the increased shaft speed increases both the turbine shaft power and the power consumption by the compressor (Fig. 10b). Also, the pressure ratios of the turbine and compressor (Fig. 13c) and the flow rate of the He–Xe working fluid in the CBC loops (Fig. 13b) increase rapidly, almost linearly with time. The simultaneously increasing reactor thermal power (Fig. 9b) and turbine inlet temperature (Fig. 10a) increase the turbine shaft power faster than the power consumed by the compressor in the UNM-BRU-1 units. Eventually, the turbine power equals that demanded by the compressor, marking the end of the motoring phase of the UNM-BRU-1 units in the $S^{\wedge}4$-CBC power system. This occurs 32 min into the startup transient (Figs. 10c and 11).

The oscillations in the motoring shaft power in Fig. 11 mimic those of the reactor thermal power and the turbine inlet temperature (Figs. 9b and 10a). The continued increases in the reactor thermal power and the turbine inlet temperature result in a positive and increasing shaft power, with the UNM-BRU-1 units supplying power to the electrical load. The temperature of the He–Xe binary mixture at the inlet of the BRU compressor, however, changes very little as the reactor thermal power increases (points 5–7 in Fig. 10a), until reaching steady-state, full-power operation (point 7).

After the UNM-BRU-1 shaft speed reaches and is maintained constant at 45 krpm, 90 min into the startup transient (point 5 in the figures), the reactor thermal power is 305 kW_{th} and the corresponding total external reactivity insertion into the $S^{\wedge}4$ reactor core is +\$0.89 (Fig. 9). The corresponding turbine and compressor inlet temperatures are 766 and 366 K (Fig. 10a), the turbine mechanical power and the compressor power consumption in each UNM-BRU-1 unit are 79.3 and 69.6 kW (Fig. 10b), and the shaft net mechanical power and the electrical power generated by each UNM-BRU-1 unit are 4.2 kW and 4.0 kW_e, respectively (Fig. 10c). In addition, the turbine and compressor pressure ratios reach their highest values of 1.44 and 1.52 (Fig. 13c), and the flow rate of the He–Xe working fluid through the turbine is 1.67 kg/s, versus 1.80 kg/s at steady-state, nominal full-power operation (point 7 in Fig. 13b).

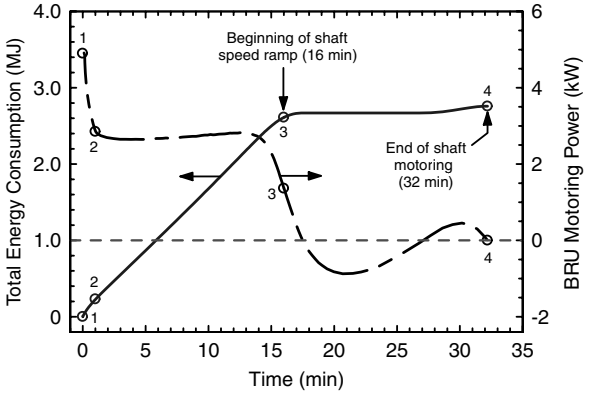

Fig. 11 UNM-BRU-1 operation parameters in the motoring period of UNM-BRU-1 units.

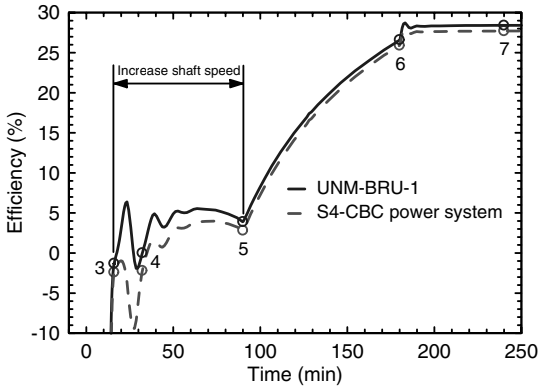

Fig. 12 Thermal efficiencies of the UNM-BRU-1 and $S^{\wedge}4$-CBC power system.

The calculated transient values of the thermal efficiencies of the UNM-BRU-1 and the power system are compared in Fig. 12. During the motoring phase of the UNM-BRU-1 units, which ends 32 min into the startup transient, these efficiencies are negative because the net mechanical power of the BRU shaft is negative. Following the end of the shaft motoring period (point 4 in the figures), the net mechanical power of the UNM-BRU-1 shaft and, hence, the thermal efficiency, become positive (Fig. 12). The system's thermal efficiency is always lower than that of the UNM-BRU-1, becoming positive 35 min into the startup transient. The lower system thermal efficiency is because a fraction of the electrical power generated by each UNM-BRU-1 is used to operate the ALIP for circulating the liquid NaK-78 in the heat rejection loop (Fig. 1). Each ALIP consumes 1.1 kW_e, reducing the system's total electrical power output by 3.3 kW_e.

During the ramp phase of UNM-BRU-1 shaft speed, from point 4 to point 5 in the figures, the thermal efficiencies of the UNM-BRU-1 and the $S^{\wedge}4$-CBC power system are nearly constant at 4% and 3%, respectively, while the mechanical powers of the UNM-BRU-1 turbine and compressor increase with time (Fig. 10b). Once the shaft speed reaches and is maintained constant at 45 krpm, the thermal efficiencies of the UNM-BRU-1 and the power system increase rapidly as the reactor thermal power and both the turbine inlet temperature and mechanical power increase, while the compressor mechanical power requirement remains nearly constant (Fig. 10b). At steady-state, nominal operation at full power, each UNM-BRU-1 delivers 44.7 kW_e and operates at a thermal efficiency of 28.5%, while the power system nets $3 \times 43.6 = 130.8$ kW_e and operates at a slightly lower thermal efficiency of 27.8% (Figs. 12 and 16).

The DynMo-CBC model of the $S^{\wedge}4$-CBC power system also calculates the changes in the bleed fraction x of the He–Xe working fluid at the exit of the compressor for cooling the rotating shaft bearings and the electrical generator in the UNM-BRU-1 unit (Figs. 1 and 13b). The bled working fluid removes the shaft mechanical losses and the generator electrical losses before mixing with the gas

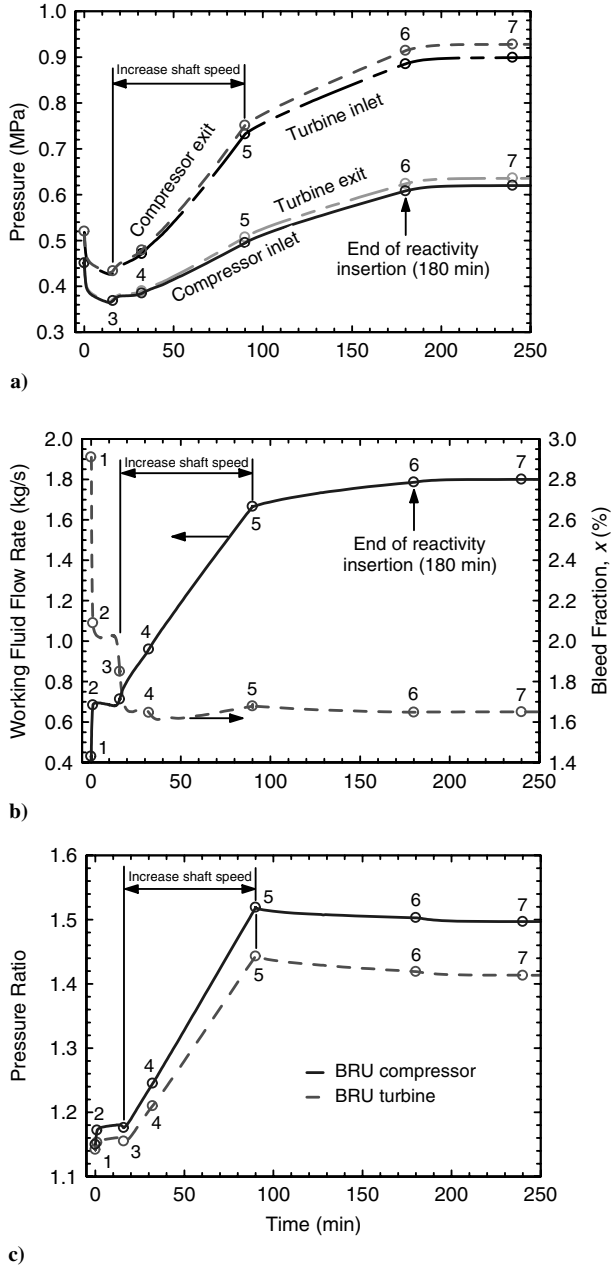

Fig. 13 Flow rate and pressures in the CBC loops during startup of *S* ^ 4-CBC power system.

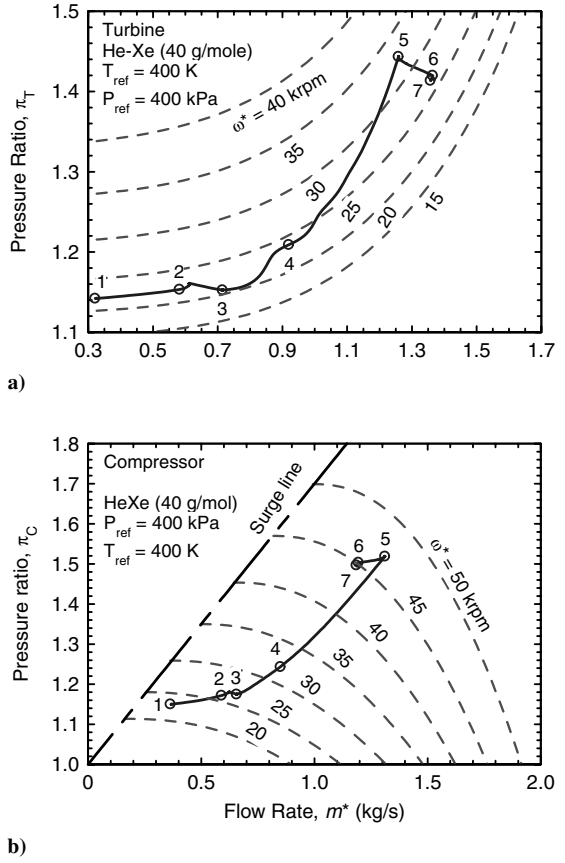

Fig. 14 Operation paths of UNM-BRU-1 turbine and compressor during startup of *S* ^ 4-CBC power system.

exiting the turbine (Figs. 1 and 16). As shown in Fig. 13b, the bleed fraction of the He–Xe working fluid at the exit of the UNM-BRU-1 compressor decreases during the startup transient of the *S* ^ 4-CBC power system, from an initial value of 2.9% of the total flow rate of the He–Xe gas working fluid in the gas cooler to 1.65% at steady-state, full power operation at a reactor thermal power of 471 kW_{th}. During the shaft speed ramp phase in the startup transient, the flow rate of the He–Xe binary mixture in the bleed line increases linearly from 0.0134 kg/s (point 3) to 0.028 kg/s (point 5 in Fig. 13b), driven by the difference in pressure between the compressor and the turbine exits (Fig. 13a). It then increases steadily, but at a much lower rate to a steady-state, full power value of 0.302 kg/s (point 7 in Fig. 13b).

As shown in Fig. 13a, the pressures in the CBC loop increase with time during the startup transient, as the reactor thermal power and the average temperature of the circulating He–Xe binary gas mixture increase. The pressures at the exit of the compressor and the inlet of the turbine of the UNM-BRU-1 increase faster than those at the exit of the gas cooler and the inlet of the compressor (Figs. 1 and 13a). This is because the compressor pressure ratio increases as the shaft speed and the mass flow rate of the He–Xe working fluid in the CBC loop increase (Figs. 7b, 13b, and 13c). At steady-state, full-power operation of the *S* ^ 4-CBC power system (point 7 in the figures), the gas pressure at the exit of the UNM-BRU-1 compressor reaches its nominal design value of 0.928 MPa [26]. The pressure at the turbine inlet is lower than at the compressor exit by the pressure losses through the cold leg of the recuperator (6.4 kPa, or 0.6% of the total inlet pressure) and in the *S* ^ 4 reactor (23.5 kPa, or 2.5% of the total inlet pressure). Similarly, the pressure at the compressor inlet is lower than at the exit of the turbine by the pressure losses in the hot leg of the recuperator (9.2 kPa, or 1.5% of the total inlet pressure) and in the gas cooler (7.3 kPa, or 1.0% of the total inlet pressure, Figs. 13a).

C. Operation Maps of Brayton Rotating Unit-1 Turbine and Compressor

The used operation design maps of the radial inflow turbine and centrifugal compressor of the UNM-BRU-1 [26] are shown in Figs. 14a and 14b, along with the actual operational paths during the startup procedures of the *S* ^ 4-CBC space power system. The mass flow rate of the He–Xe working fluid and the rotation speed of the UNM-BRU-1 shaft are normalized (see Nomenclature), using reference temperature and pressure of 400 K and 400 kPa. For a fixed value of the normalized shaft speed ω^* the turbine pressure ratio increases rapidly as the normalized mass flow rate of the He–Xe working fluid in the CBC loop m^* increases (Fig. 14a). The higher the rotation shaft speed, the higher the pressure ratio of the radial-inflow turbine.

The operation path of the UNM-BRU-1 turbine during the startup transient, indicated by the bold solid curve in Fig. 14a, reflects the combined contributions due to the changes in the He–Xe flow rate in the turbine and the turbine inlet pressure and temperature. The increase in the shaft rotation speed of the UNM-BRU-1, and the resulting increase in m^* following the radiator deployment, explain the rapid decrease in the system pressure (from point 1 to 3 in

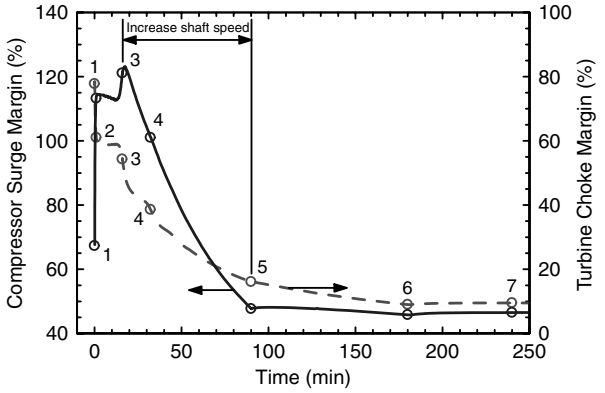

Fig. 15 Compressor surge margin and turbine choke margin during startup of $S\hat{}4$ CBC power system.

Fig. 13a). This is because the heat rejection by the radiator panels lowers the temperature of the He–Xe binary gas mixture in the CBC loops of the power system. The linear increase in the shaft rotation speed from point 3 to 5 increases the pressure ratio and the mass flow rate of the He–Xe working fluid in the CBC loops (Figs. 13b and 13c). From points 5 to 7, the UNM-BRU-1 shaft speed is kept constant at 45 krpm, the pressure ratio of the turbine decreases (Fig. 13a), and the mass flow rate of the He–Xe working fluid in the CBC loop increases slowly (Fig. 13b) to their respective steady-state, full-power operation values.

As shown in Fig. 14b, the surge limit of the UNM-BRU-1 centrifugal compressor is nearly linear with increasing the flow rate of the He–Xe working fluid. The lines of constant normalized shaft speeds intersect the compressor surge limit line and the pressure ratio decreases rapidly as either the mass flow rate of the He–Xe working fluid increases or the rotation speed of the UNM-BRU-1 shaft decreases. The operational path of the UNM-BRU-1 compressor during the demonstrated startup transient, indicated by the bold solid curve in Fig. 14b, shows that following the radiator deployment and the subsequent decrease in the CBC loop pressure there is an increase in the normalized mass flow rate of the He–Xe working fluid, between points 1 and 3. The slow decrease in the normalized mass flow of the He–Xe working fluid, from point 5 to 7 when the system reaches steady-state full-power operation, is caused by the increase in the pressure at the inlet of the UNM-BRU-1 compressor (Fig. 13a). Though point 1, at the beginning of the startup procedures, appears closest to the compressor surge line in Fig. 14b, it actually corresponds to a design operation margin of 67%, compared to 47% at the steady state, full power operation (point 7 in Figs. 14b and 15). The compressor design operation surge margin increases as the difference between the actual mass flow rate of the He–Xe working fluid and that corresponding to the surge limit, for the same normalized shaft speed, increases.

Following the deployment of the radiator and the subsequent cooling of the CBC loops, the design surge margin of the UNM-BRU-1 compressor increases rapidly to as much as 121% at point 3, as the normalized flow rate of the He–Xe working fluid increases, but the compressor pressure ratio remains essentially constant (Figs. 13c and 15). During the ramp phase of the UNM-BRU-1 shaft speed (points 3 to 5) the compressor operation margin from the surge limit decreases rapidly to 48%, and the compressor operation path becomes nearly parallel to the surge limit line (Fig. 14b).

The UNM-BRU-1 turbine choking margin is also indicated in Fig. 15. It is the difference between the maximum Mach number in the turbine and the sonic limit of unity. Once the He–Xe gas flow through the turbine reaches the sonic limit, choking prevents any further increase in the flow rate through the turbine. Because the normalized mass flow rate of the He–Xe working fluid through the turbine m^* is proportional to the Mach number (see Nomenclature), the choke condition in the UNM-BRU-1 turbine is well identified by a constant value of $m^* = 1.50$. The turbine choking margin, therefore, exhibits an opposite trend to that of the normalized mass flow rate (see Figs. 14a and 15). The turbine choking margin decreases with increasing flow rate. Its highest value of 80% occurs at the beginning of the startup transient, when the flow rate of the He–Xe working fluid through the CBC loop is low (Fig. 13b). The lowest choking margin of 10% (Fig. 15), corresponding to a Mach number of 0.90, occurs at steady-state, full-power operation of the power system.

D. Power System Performance

Between 90 (point 5 in the figures) and 180 min (the end of the startup procedures, point 6 in the figures) in the simulated startup transient of the $S\hat{}4$-CBC power system, the rotation speed of the UNM-BRU-1 shaft is maintained constant at 45 krpm, while the external reactivity insertion into the reactor core continued at a constant rate of 1.04 ¢/ min. At the end of the startup transient (point 6 in the figures), the total reactivity insertion into the reactor core is +\$1.79. At steady-state full-power operation of the power system, the thermal power of the $S\hat{}4$ reactor is 471 kW_{th} (Fig. 9b), the turbine inlet temperature is 1149 K (Fig. 10a), and the compressor inlet temperature and exit pressure are 400 K and 0.928 MPa (Figs. 13a and 16). At these conditions, the UNM-BRU-1 turbine and compressor operate at pressure ratios of 1.414 and 1.50 and have polytropic efficiencies of 94.1 and 86.3%, respectively (Figs 13c and 16). Excluding the power consumption by the three ALIPs for circulating the liquid NaK-78 in the heat rejection loops and the ducts

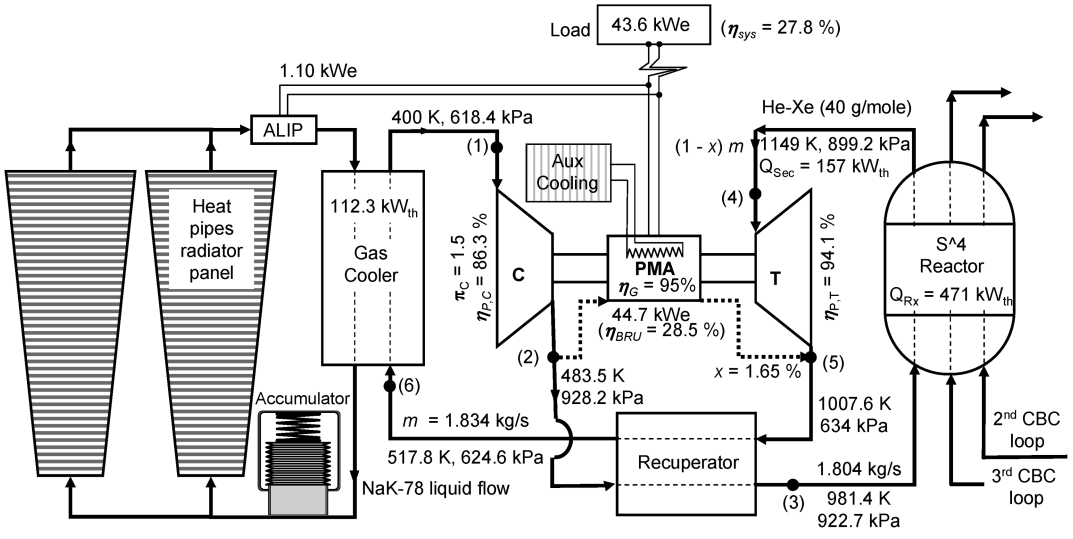

Fig. 16 Full-power, steady-state operation parameters in one loop of $S\hat{}4$-CBC space power system.

of the radiator panels, each UNM-BRU-1 generates a net electrical power of 44.7 kW_e at a thermal efficiency of 28.5% (Figs. 10c and 16). After accounting for the electric power consumption by the three ALIPs (each ALIP consumes 1.1 kW_e), the net electrical power of the $S\hat{}4$-CBC space power system with three CBC loops is 130.8 kW_e at a thermal efficiency of 27.8% (Fig. 16). The developed design of the UNM-BRU-1 has been optimized for these operation conditions [26].

At the system's steady-state full-power operation delineated in Fig. 16, each CBC loop rejects a total of 112.3 kW_{th} to the circulating liquid NaK-78 in the heat rejection loop, to be equally rejected into space by two water heat pipe radiator panels. The corresponding specific mass of the UNM-BRU-1 is as small as $\sim$1.16 kg/kW_e and the Co–Sm permanent magnet of the BRU alternator is cooled below 500 K using an auxiliary heat pipes radiator. The bleed fraction of the He–Xe working fluid at the exit of the UNM-BRU-1 compressor, for cooling the rotating shaft, compressor and turbine disks and bearings, and the electrical alternator, is 1.65% (or 30.26 g/s, Figs. 13b and 16).

The $S\hat{}4$ reactor steady-state thermal power of 471 kW_{th} is determined based on detailed thermal-hydraulic and computational fluid dynamic analyses [10]. Therefore, increasing this thermal power requires redesigning the reactor and performing detailed neutronic and thermal analyses. On the other hand, the power system's electrical power could be intermittently decreased below the nominal value of 130.8 kW_e (Fig. 16), in order to meet a specific power requirement profile for a space mission. This may be done in two ways:

1) Lower the steady-state electrical power generated by the $S\hat{}4$-CBC space power system by decreasing the thermal power of the reactor and the flow rate of the He–Xe reactor coolant and CBC working fluid commensurate with the decrease in the reactor thermal power, while operating at the same compressor and turbine inlet temperatures of 400 and 1149 K (Fig. 16) and the UNM-BRU-1 shaft speed of 45 krpm.

2) Maintain the reactor's steady-state thermal power at its nominal design value 471 kW_{th} and decrease the inlet temperature to the UNM-BRU-1 turbine to $<$1000 K, while operating at the same compressor inlet temperature of 400 K and the UNM-BRU-1 shaft speed of 45 krpm.

The first approach for decreasing the electrical power of the $S\hat{}4$-CBC power system decreases the depletion of fissile and the accumulation of fission products in the reactor core and increases the operating life of the reactor and the power system. The second approach does not effectively change the current nominal operation life of the $S\hat{}4$ reactor and the power system ($\sim$12 years) [8–10] but decreases the UN fuel temperature and hence, the fission gas release and fuel swelling. In addition, because of the low turbine inlet temperature (900 K), it would be possible to use a conventional steel structure. These attributes will increase the operation reliability and effectively reduce the development cost and the time to actual deployment of the $S\hat{}4$ power system. Either option or a combination of the above options for changing the electrical power of the $S\hat{}4$-CBC space reactor power systems will be investigated and results reported in a future article.

E. Uncertainties in Reported Results

An important consideration in the dynamic simulation of a space reactor power system is to provide estimates of the uncertainties in the results. However, in the absence of a canonical case or actual system performance results, the authors rely on the validation results of the developed components' models, when possible, and the analytical validation of the governing equations in the models of the components and of the closed CBC loop, such as satisfying the overall momentum and energy balance equations and accounting for the various losses.

The model of the CBC units in DynMo-CBC has been validated by comparing its predictions with reported performance results of earlier NASA BRU units. These BRUs had been tested successfully in a simulated space environment for more than 35,000 hrs without failure. The predictions of the BRU model are within only a few percent ($<$3%) of the reported performance results for the NASA BRUs [26].

The reactivity feedback coefficients due to temperature and the depletion of fissile in the UN fuel with an operation life of the $S\hat{}4$ reactor have been calculated using the Monte Carlo particle transport and fuel depletion code (MCNPX, [9,10]). Thus, calculated reactivity feedback coefficients for the $S\hat{}4$ reactor core would be subject to the statistical uncertainties in the code calculations, which could be as much as 3–5%. It is worth noting, however, that MCNPX calculations account for the changes in the UN fuel volume and density and in the densities of the various structure materials in the reactor, but neglect the overall thermal expansion of the $S\hat{}4$ solid core. This assumption, although conservative, could introduce an additional uncertainty of $\sim$1%–2%. Other uncertainties in the reported results could be caused by those in the physical and thermal properties of the UN fuel and structure materials and the dimensions of the piping in the CBC loop and the various system components. Thus, the primary emphasis of this paper has been on demonstrating the dynamic simulation of such a complex space reactor power system, rather than on the accuracy of the simulation results. It would be possible to validate the latter when actual performance results become available.

V. Conclusions

A dynamic simulation model (DynMo-CBC) of the $S\hat{}4$-CBC space power system for generating a nominal steady-state power of 130.8 kW_e at a thermal efficiency of 27.8% is developed based on the SIMULINK® platform. The $S\hat{}4$-CBC space reactor power system has no single-point failures in reactor cooling and energy conversion and has a nominal operation lifetime of $\sim$12 years. The $S\hat{}4$ reactor core is comprised of three sectors that are thermally and neutronically coupled but hydraulically independent. Each sector is thermal-hydraulically coupled to a separate CBC loop with a UNM-BRU-1 unit and a heat rejection loop with circulating liquid NaK-78 and two water heat pipe radiator panels. The reactor coolant and CBC working fluid is a He–Xe binary gas mixture with a molecular weight of 40 g/mol.

The capabilities of the DynMo-CBC are demonstrated in this paper by simulating a transient startup of the $S\hat{}4$-CBC power system from an initial uniform temperature of 400 K to full-power steady-state operation at a reactor thermal power of 471 kW_{th}, UNM-BRU-1 shaft rotation speed of 45 krpm, and turbine and compressor inlet temperatures of 1149 K and 400 K. The rotation speed of the UNM-BRU-1 is adjusted at the specified values in the startup procedures using a PID controller. During the simulated system's startup, the UNM-BRU-1 compressor has at least 46% operation margin from the surge limit and the turbine has at least 10% operation margin from choke limit.

The developed design of the UNM-BRU-1 has been optimized for nominally operating at a thermal efficiency of 28.5% and generating 44.7 kW_e when the thermal power input to the turbine is 157 kW_{th}, the shaft rotation speed is 45 krpm, and the compressor and turbine inlet temperatures are 400 and 1149 K [26]. The UNM-BRU-1 has a nominal specific mass of $\sim$1.16 kg/kW_e and employs an alternator with an efficiency of 95% and Co-Sm permanent magnet that is cooled below 500 K using an auxiliary heat pipes radiator.

The simulated startup procedures of the $S\hat{}4$-CBC space reactor power system took 4 hours to complete. At full-power, steady-state operation of the power system, the pressure ratios of the UNM-BRU-1 turbine and compressor are 1.414 and 1.50 and polytropic efficiencies are 94.1 and 86.3%, respectively. After accounting for the electric power consumption by the three ALIPs for circulating the liquid NaK-78 in the heat rejection loops and the six radiator panels, the power system's nominal electrical power is 130.8 kW_e and the corresponding thermal efficiency is 27.8%. The results demonstrated the transient capabilities of the DynMo-CBC, which could be easily used to simulate transient operation of other space reactor power systems with CBC energy conversion.

Acknowledgment

This research is sponsored by the University of New Mexico's Institute for Space and Nuclear Power Studies.

References

[1] El-Genk, M. S., "High-Energy Utilization, Dual-Mode System Concept for Mars Missions," *Journal of Propulsion and Power*, Vol. 17, No. 2, 2001, pp. 340–346.

[2] El-Genk, M. S., "Space Nuclear Reactor Power System Concepts with Static and Dynamic Energy Conversion," *Energy Conversion and Management*, Vol. 49, No. 3, 2008, pp. 402–411. doi:10.1016/j.enconman.2007.10.014

[3] El-Genk, M. S., "Space Reactor Power Systems with No Single Point Failures," *Nuclear Engineering and Design*, Vol. 238, No. 9, 2008, pp. 2245–2255. doi:10.1016/j.nucengdes.2008.02.026

[4] El-Genk, M. S., and Tournier, J.-M., "DynMo-TE: Dynamic Simulation Model for Space Reactor Power Systems with Thermoelectric Converters," *Nuclear Engineering and Design*, Vol. 236, No. 23, 2006, pp. 2501–2529. doi:10.1016/j.nucengdes.2006.03.004

[5] Hatton, S. H., and El-Genk, M. S., "Sectored Compact Space Reactor (SCORE) Concepts with a Supplementary Lunar Regolith Reflector," *Progress in Nuclear Energy*, Vol. 51, No. 1, 2009, pp. 93–108. doi:10.1016/j.pnucene.2007.12.003

[6] El-Genk, M. S., and Tournier, J.-M., "SAIRS–Scalable AMTEC Integrated Reactor Space Power System," *Progress in Nuclear Energy*, Vol. 45, No. 1, 2004, pp. 25–69. doi:10.1016/j.pnucene.2004.08.002

[7] El-Genk, M. S., Hatton, S., Fox, C., and Tournier, J.-M., "SCoRe: Concepts of Liquid Metal Cooled Space Reactors for Avoidance of Single-Point Failure," *Proceedings of Space Technology and Applications International Forum (STAIF-05)*, edited by M. S. El-Genk, AIP Conference Proceedings, 746, American Institute of Physics, Melville, NY, 2005, pp. 473–484.

[8] King, J. C., and El-Genk, M. S., "Thermal-Hydraulic Analyses of the Submersion-Subcritical Safe Space ($S^\wedge 4$) Reactor," *Proceedings of Space Technology and Applications International Forum (STAIF-07)*, edited by M.S. El-Genk, AIP Conference Proceedings No. 880, American Institute of Physics, Melville, NY, 2007, pp. 261–270.

[9] King, J. C., and El-Genk, M. S., "Temperature and Burnup Reactivities and Operational Lifetime for the Submersion Subcritical Safe Space $S^\wedge 4$ Reactor," *Nuclear Engineering and Design*, Vol. 237, No. 5, 2007, pp. 552–564. doi:10.1016/j.nucengdes.2006.07.008

[10] King, J. C., and El-Genk, M. S., "Thermal-Hydraulic and Neutronic Analyses of the Submersion-Subcritical, Safe Space $S^\wedge 4$ Reactor," *Nuclear Engineering and Design*, Vol. 239, 2009, pp. 2809–2819. doi:10.1016/j.nucengdes.2009.09.021

[11] Metzger, J. D., and El-Genk, M. S., "Application of a Model-Reference Adaptive Controller with Selective State-Variable Weighting to an SP-100 Space Nuclear Power System," *Journal of Propulsion and Power*, Vol. 8, No. 5, 1992, pp. 1093–1102.

[12] Richard, T. W., Neal, J. S., Brittain, C. R., and Mullens, J. A., "Autonomous Control Capabilities for Space Reactor Power Systems," *Proceedings of Space Technology and Applications International Forum (STAIF-04)*, edited by M. S. El-Genk, AIP Conference Proceedings, 699, American Institute of Physics, Melville, NY, 2004, pp. 631–638.

[13] Na, M. G., and Upadhyaya, B. R., "Model Predictive Control of an SP-100 Space Reactor using Support Vector Regression and Genetic Optimization," *IEEE Transactions on Nuclear Science*, Vol. 53, No. 4, 2006, pp. 1318–2327. doi:10.1109/TNS.2006.876517

[14] El-Genk, M. S., and Seo, J. T., "SNPSAM: Space Nuclear Power System Analysis Model," *Space Nuclear Power Systems 1986*, edited by M. El-Genk, and M. Hoover, Vol. 5, Orbit Book Co., Inc., Malabar, FL, 1987, pp. 111–123.

[15] El-Genk, M. S., and Seo, J. T., "A Study of the SP-100 Radiator Heat Pipes Response to External Thermal Exposure," *Journal of Propulsion and Power*, Vol. 6, No. 1, 1990, pp. 69–77.

[16] El-Genk, M. S., and Rider, W. J., "Reliability and Vulnerability Studies of the SP-100 Dual-Loop Thermoelectric-Electromagnetic Pumps," *Journal of Propulsion and Power*, Vol. 6, No. 3, 1990, pp. 305–314.

[17] El-Genk, M. S., Seo, J. T., and Buksa, J. J., "Load Following and Reliability Studies of an Integrated SP-100 System," *Journal of Propulsion and Power*, Vol. 4, No. 2, 1988, pp. 152–156. doi:10.2514/3.23043

[18] Paramonov, D. V., and El-Genk, M. S., "Development and Comparison of a TOPAZ-II System Model with Experimental Data," *Journal of Nuclear Technology*, Vol. 108, No. 2, 1994, pp. 157–170.

[19] El-Genk, M. S., Xue, H., and Paramonov, D., "Transient Analysis and Start-up Simulation of a Thermionic Space Nuclear Reactor System," *Journal of Nuclear Technology*, Vol. 105, No. 1, 1993, pp. 70–86.

[20] Mondt, J. F., and Truscello, V. C., "SP-100 Technical Summary Rept.," Jet Propulsion Lab. JPL D-11818, Pasadena, CA, 1994.

[21] Demuth, S. F., "SP-100 Space Reactor Design," *Progress in Nuclear Energy*, Vol. 42, No. 3, 2003, pp. 323–359. doi:10.1016/S0149-1970(03)90003-5

[22] Tournier, J.-M., and El-Genk, M. S., "Bellows-Type Accumulator for Liquid Metal Loops of Space Reactor Power Systems," *Proceedings of Space Technology and Applications International Forum (STAIF-06)*, edited by M. S. El-Genk, AIP Conference Proceedings, 816, American Institute of Physics, Melville, NY, 2006, pp. 730–742.

[23] Tournier, J.-M., and El-Genk, M. S., "Liquid Metal Loop and Heat Pipes Radiator for Space Reactor Power Systems," *Journal of Propulsion and Power*, Vol. 22, No. 5, 2006, pp. 1117–1134. doi:10.2514/1.20031

[24] SIMULINK® 6.1, http:/www/mathworks.com/products/simulink [retrieved 15 Sept. 2008].

[25] El-Genk, M. S., and Schriener, T. M., "Performance and Radiological Analyses of Space Reactor Power System Deployed into a 1000–3000 km Earth Orbit," *Progress in Nuclear Energy*, Vol. 52, 2010, pp. 236–248. doi:10.1016/j.pnucene.2009.06.014

[26] Gallo, B. M., and El-Genk, M. S., "Brayton Rotating Units for Space Reactor Power Systems," *Energy Conversion and Management*, Vol. 50, No. 9, 2009, pp. 2210–2232. doi:10.1016/j.enconman.2009.04.035

[27] El-Genk, M. S., and Tournier, J.-M., "High Temperature Water Heat Pipes Radiator for a Brayton Space Reactor Power System," *Proceedings of Space Technology and Applications International Forum (STAIF-06)*, edited by M. S. El-Genk, AIP Conference Proceedings, 813, American Institute of Physics, Melville, NY, 2006, pp. 716–729.

[28] Polzin, K. A., "Liquid-Metal Pump Technologies for Nuclear Surface Power," NASA Rept. No. NASA/TM-2007-214851, NASA Marshall Space Flight Center, March 2007.

[29] El-Genk, M. S., and Tournier, J.-M., "Noble Gas Binary Mixtures for Closed Brayton Cycle Space Reactor Power Systems," *Journal of Propulsion and Power*, Vol. 23, No. 4, 2007, pp. 863–873. doi:10.2514/1.27664

G. Spanjers
Associate Editor